Singularity Detection and Characterization with Complex-Valued Wavelets and their Applications

†‡Chun-Liang Du and †Wen-Liang Hwang
†Institute of Information Science, Academia Sinica, Taiwan
‡Computer & Communications Research Laboratories, ITRI, Taiwan

Abstract

We prove that the wavelet modulus maxima with a complex-valued wavelet can detect and characterize singularities. This can be regarded as an extension of the previous wavelet modulus work in [13] with a real wavelet. The ridges of wavelet transforms are the places in the time-frequency plane where the local energies of a signal are mostly concentrated. We show that based on the ridges of the wavelet transforms, the osciallating singularities are better located and their oscillating components are better characterized than they are based on the general maxima of real-valued wavelet transforms. We demonstrate potential applications of these techniques.

Key Words: Continuous Wavelet Transform, Wavelet Modulus Maxima, Singularity, Instantaneous Frequencies

SP EDICS: 2-SPTM

1 Introduction

Wavelet analysis has emerged in recent years as a methodology for solving problems in many different areas. Among these applications, it is believed that the wavelet approach can achieve tremendous success in the detection and characterization of the irregular structures of a signal. These are usually isolated singularities and, thus, can be characterized by their Lipschitz exponents, or as a distribution of singularities and measured based on their spectrum [2]. Singularities also carry important information in images. They correspond to the locations of intensity discontinuities in an image and are usually referred to as "edges" in the image [14]. In planar objects, the curvature discontinuities of the contour boundaries are primitive with respect to description and recognition of the shapes [4].

Irregular behavior of a signal can be characterized by wavelet transforms. Some pioneer works were reported in [10][15]. We rephrase one of the results in Appendix A. A wavelet can be either real-valued or complex-valued. We use the term real-valued wavelet transform (modulus maxima) or complex-valued wavelet transform (modulus maxima) to denote the wavelet transform (modulus maxima) of a real function obtained with a real-valued wavelet or a complex-valued wavelet, respectively. It was shown in [13] that the real-valued wavelet modulus maxima can detect all the singularities and characterize the singularities. Also, the real-valued wavelet modulus maxima carry as just much information about a signal since a close approximation of a signal can be numerically constructed only from the information contained in the real-valued wavelet modulus maxima [12]. However, there are no similar results for singularity detection and characterization based on complex-valued wavelet modulus maxima.

On the other hand, the complex-valued wavelet transform of a signal has applications in many fields. A popular complex-valued progressive wavelet can be obtained by taking the imaginary part of the wavelet such that it is the Hilbert transform of the real part of the wavelet. This wavelet responds only to the non-negative frequencies of a given signal and, thus, produces a transform whose

modulus are less oscillatory than is the case for one obtained based on a real-valued wavelet. Complex-valued wavelet transforms have been widely used to detect and characterize the instantaneous frequencies of a signal and to analyze a textured image [11][7][8]. A concise but not complete representation of it is the ridges of the complex-valued wavelet transform. The ridges mark the places in the time-frequency plane where most of the local energies of a signal are concentrated. One can detect ridges from either the phase or the magnitude of a complex-valued wavelet transform [6]. A signal's instantaneous frequencies can be approximately identified from the real-valued wavelet modulus based on the notion of the general maxima, which are the places that have the largest modulus along maxima lines (see Definition in later section) [13]. However, compared to the ridges, the general maxima does not provide as elegant a method for detecting and characterizing instantaneous frequencies.

The major contribution of this paper is to show that one is able to use complex-valued wavelet modulus maxima, like real-valued wavelet modulus maxima, to detect and characterize singularities. We will present some mathematical results similar to those given by Mallat and Hwang [13] with a complex-valued wavelet. Once the singularity can be detected and characterized from complex-valued wavelets, one can envision the possible effectiveness of processing instantaneous frequencies as well as singularities simultaneously based on the modulus of a complex-valued wavelet transform.

The paper is organized as follows. Section 2 contains some background material on complex-valued wavelet transform. In section 3, we will review the results of singularity processing using real-valued wavelet modulus maxima and then will present our results from the complex-valued wavelet modulus maxima. In section 4, we will introduce potential applications of our results. In pattern recognition, invariant features are important in indexing objects. We characterize the curvature singularity created by spiral-like curves. We propose a segmentation method which can partition the contour of a planar shape into subcomponents by means of either curvature singularities or ridges. There are other potential applications which are not discussed in this article. Finally, the last section will give conclusions.

2 Complex-Valued Wavelets

We will review the continuous wavelet transform with a complex-valued wavelet. The continuous wavelet transform was first introduced by Morlet and Grossmann [9]. Let $\Psi(x)$ be a complex-valued function. The function $\Psi(x)$ is said to be a complex-valued wavelet if its Fourier transform $\hat{\Psi}(\omega)$ satisfies

$$\int_0^{+\infty} \frac{|\hat{\Psi}(\omega)|^2}{\omega} d\omega = \int_{-\infty}^{0} \frac{|\hat{\Psi}(\omega)|^2}{\omega} d\omega = C_\Psi < +\infty. \tag{1}$$

The wavelet transform of a function $f(x) \in \mathcal{L}^2(R)$ is defined by

$$\mathcal{W}f(s,x) = f * \Psi_s(x), \tag{2}$$

where $\Psi_s(x) = \frac{1}{s}\Psi(\frac{x}{s})$. A wavelet $\Psi(x)$ is said to have n vanishing moments if and only if for all positive integer $k < n$, it satisfies

$$\int_{-\infty}^{+\infty} x^k \Psi(x) dx = 0. \tag{3}$$

If we use a complex-progressive wavelet of the type $\Psi(x) = (1+i\mathcal{H})\psi(x)$, where $\psi(x)$ is a real wavelet and $\mathcal{H}$ denotes the Hilbert transform, then we restrict the wavelet analysis in the real Hardy space:

$$\mathcal{H}^2(R) = \{\mathcal{W}f(s,x) \in \mathcal{L}^2(R); \hat{\mathcal{W}}f(s,\omega) = 0 \quad \text{for} \quad \omega \leq 0 \quad \text{and for all} \quad s > 0\}.$$

The wavelet transform is invertible, and $f(x)$ is recovered with

$$f(x) = Re\{\frac{1}{C_\Psi} \int_{0^+}^{+\infty} \int_{-\infty}^{+\infty} \mathcal{W}f(s,u) \bar{\Psi}_s(u-x) du \frac{ds}{s}\}, \tag{4}$$

where $\bar{\Psi}_s(x)$ denotes the complex conjugate of $\Psi_s(x)$.

There are several interesting complex-valued progressive wavelets, and they have been used in a wide variety of applications. For example, the so-called Cauchy wavelet[1] $\Psi(x) = \frac{1}{2\pi}\frac{1}{(1-ix)^2}$ has been used in quantum mechanics. The Morlet wavelet $\Psi(x) = e^{-\frac{x^2}{2\sigma^2}} e^{i\omega_0 x}$ has been used extensively in detecting instantaneous frequencies and in analyzing textured images [7][11][8]. Strictly speaking,

the Morlet wavelet is not a wavelet because it is not of integral zero. However, for large enough ω_0 (larger than 5 in practice), the integral of $\Psi(x)$ is small enough to ensure that for all practical purposes, it can be used numerically as if it were a wavelet. A very popular type of wavelet in computer vision is the derivative of the Gaussian with the following formula:

$$\psi_n(x) = -\frac{d^n}{dx^n} e^{-\frac{x^2}{2}}. \tag{5}$$

These wavelets can be easily turned into progressive wavelets by canceling their negative frequencies by means of Hilbert transform $\mathcal{H}$, i.e., by considering $\Psi_n(x) = (1 + i\mathcal{H})\psi_n(x)$. Then, the frequency response will be

$$\hat{\Psi}_n(\xi) = K_n \xi^n e^{-\frac{\xi^2}{2}} \chi_{(0,\infty)}(\xi),$$

where $\chi_{(0,\infty)}(\xi)$ denotes the Heaviside step function, which is equal to 1 when $\xi > 0$ and to 0 otherwise, and K_n denotes a normalization constant. The parameter n gives different numbers of vanishing moments of wavelets. When studying singularity analysis with wavelets, the number of vanishing moments is very important. A real-valued wavelet becomes more oscillatory as the number of vanishing moments increases. Fig. 1 shows examples of this wavelet with $n = 1$ and $n = 2$ with the real part given in (a), the imaginary part in (b), the amplitude in (c) and the phase in (d), respectively.

3 Singularity Detection and Characterization with Modulus Maxima of a Complex-Valued Wavelet

Much information about a signal can be extracted from its singularities. We usually use the Hölder exponent as a measurement of the strength of a singularity. It has been shown that the Hölder exponent of a local singularity can be characterized by the wavelet transforms. One can find related results in [10][15][16] for further reference. Nevertheless, Mallat and Hwang [13] showed that the Hölder exponent can also be computed with the restriction of the wavelet transforms,

$\mathcal{W}f(s,x)$, placed on their local modulus maxima at each scale s. However, their results are valid only for the case where the wavelet is real.

In this section, we will first review some results of Mallat and Hwang regarding the modulus maxima of a real wavelet. Then, we will extend part of their results from the modulus maxima of a complex-valued wavelet. We will show that the modulus maxima of a complex-valued wavelet can also detect and characterize singularities. However, before we proceed to our results, we will first introduce some related definitions.

Definition

• If a function $f(x)$ satisfies $|f(x) - f(y)| \leq c|x-y|^{\alpha}$ with $c > 0$, $\alpha \in (0, 1]$ and $x, y \in (a, b)$, then we say that the function $f(x)$ is uniformly Lipschitz α over the interval. A function is singular at x_0 if it is not Lipschitz 1 at x_0.

• A modulus maximum is the point (s_0, x_0) where $|\mathcal{W}f(s_0, x)| < |\mathcal{W}f(s_0, x_0)|$ when x belongs to either the right or the left neighborhood of x_0, and $|\mathcal{W}f(s_0, x)| \leq |\mathcal{W}f(s_0, x_0)|$ when x belongs to the other side of the neighborhood of x_0.

• A maxima line is a connected curve of modulus maxima in the scale space (s, x).

3.1 Isolated Singularity

The following theorem was presented in [13] with a real wavelet.

Theorem 1 *Let n be a strictly positive integer. Let $\psi(x)$ be a compact support real wavelet that has n vanishing moments and is n times continuously differentiable. Let $f(x) \in \mathcal{L}^1([a, b])$.*

- *If there exists a scale $s_0 > 0$ such that for all scales $s < s_0$ and $x \in (a, b)$, and $|\mathcal{W}f(s, x)|$ has no local maxima, then for any $\epsilon > 0$ and $\alpha < n$, $f(x)$ is uniformly Lipschitz α in $(a + \epsilon, b - \epsilon)$.*

- *If $\psi(x)$ is the nth derivative of a smoothing function, then $f(x)$ is uniformly Lipschitz n on any such interval $(a + \epsilon, b - \epsilon)$.*

- *Let $x_0 \in (a, b)$. We say that $f(x)$ is uniformly Lipschitz n at x when $x \neq x_0$, and that $f(x)$ is Lipschitz α at x_0, where $\alpha < n$ is a non-integer, if and only*

if there exist a scale $s_0 > 0$ and constants C and A, such that for $x \in (a, b)$ and $s < s_0$, all the modulus maxima of $\mathcal{W}f(s, x)$ belong to a cone defined by

$$|x - x_0| \leqq Cs, \tag{6}$$

and such that at each modulus maxima (s, x) in the cone defined by (6),

$$|\mathcal{W}f(s, x)| \leqq As^{\alpha}.$$

The above theorem indicates that the wavelet modulus maxima of a real wavelet can detect all the singular points in a given interval. The maxima lines converge as the scale s decreases to all (though not limited to) the singular points in the interval, and from the values of the lines, one can characterize their Lipschitz exponents.

In order to extend the abovementioned results from a real wavelet to a complex-valued wavelet, one should place constraints on the real-part wavelet transforms and the imaginary-part wavelet transforms. For convenience, we introduce here the following definition: We say that two functions $a(x)$ and $b(x)$ are finite-deviations within a given interval I if for any subinterval (of length ϵ) of I, they can be divided into at most $M(\epsilon)$ intervals $v_1, v_2, ..., v_M$, where in each interval v_i, either $a(x) = b(x)$ for all x in v_i or $a(x) = b(x)$ at the two ends of the interval but $a(x) \neq b(x)$ for any x in between them. An example of functions which are not finite-deviations for any interval including $x = 0$ are $\cos(\frac{1}{x})$ and 0. The two functions have an unbound number of intersections for any subinterval around $x = 0$.

We will show in the following theorem that given an interval, if there is no complex-valued wavelet modulus maxima on all sufficiently small scales, and if the real and the imaginary parts of the wavelet transform in all these scales are finite-deviations, then the function is uniformly Lipschitz α, for any $\alpha < n$, in this interval.

Theorem 2 *Let n be a strictly positive integer. Let $\Psi(x)$ be a complex-valued wavelet which has compact support, has n vanishing moments and is n times continuously differentiable. Let $f(x) \in L^1([a, b])$.*

•*If there exists a scale* $s_0 > 0$ *such that for all scales* $s < s_0$ *and* $x \in (a, b)$, $|\mathcal{W}f(s,x)|$ *has no local maxima, and if the* $nth(n > 0)$ *derivatives of* $Re(\mathcal{W}f(s,x))$ *and* $Im(\mathcal{W}f(s,x))$ *are finite-deviation for each scale* s, *then for any* $\epsilon > 0$ *and* $\alpha < n$, $f(x)$ *is uniformly Lipschitz* α *in* $(a+\epsilon, b-\epsilon)$.

•*If* $\Psi(x)$ *is the* nth *derivative of a smoothing function, then* $f(x)$ *is uniformly Lipschitz* n *on any such interval* $(a+\epsilon, b-\epsilon)$.

The proof of this theorem is given in Appendix C. This theorem indicates that in order to have wavelet modulus maxima of a complex-valued wavelet $\Psi(x) = \psi_R(x) + i\psi_I(x)$ for detecting all the singular points of a function $f(x)$ as is the case with the real wavelet $\psi_R(x)$, we must choose the imaginary part of the wavelet $\psi_I(x)$ such that the real and the imaginary parts of the wavelet transform for the given function $f(x)$ are finite-deviations for all sufficiently small scales. Thus, we have the constraint between the real part and the imaginary part of a complex-valued wavelet for detection of the singularities of a given function.

The following theorem states that the wavelet modulus maxima of a complex-valued wavelet can characterize singularities.

Theorem 3 *Let* $f(x)$ *be a function, let* $x_0 \in (a, b)$ *and let the* $nth(n > 0)$ *derivative of* $Re(\mathcal{W}f(s,x))$ *and* $Im(\mathcal{W}f(s,x))$ *be finite-deviation for each scale* s. *We say that* $f(x)$ *is uniformly Lipschitz* n *at* x *when* $x \neq x_0$, *and that* $f(x)$ *is Lipschitz* α *at* x_0, *where* $\alpha < n$ *is a non-integer, if there exist a scale* $s_0 > 0$ *and constants* C *and* A, *such that for* $x \in (a, b)$ *and* $s < s_0$, *all the modulus maxima of* $\mathcal{W}f(s,x)$ *belong to a cone defined by*

$$|x - x_0| \leqq Cs, \tag{7}$$

and such that at each modulus maxima (s, x) *in the cone defined by (7),*

$$|\mathcal{W}f(s,x)| \leqq As^{\alpha}. \tag{8}$$

The proof of this theorem is similar to that in Appendix B in [13]. We sketch it in Appendix D. In order to obtain the Lipschitz exponent numerically, Equation(8) is usually rewritten as

$$log|\mathcal{W}f(s,x)| \leq log(A) + \alpha log(s). \tag{9}$$

In [13], A and α are computed by

$$\min_{A,\alpha}(\sum_{s}|log|\mathcal{W}f(s,x)| - log(A) - \alpha log(s)|^2).$$

However, it is known that estimating α by means of least squared fitting is not reliable in practice. A more robust least median of squares regression [18] is used to find A and α so as to minimize

$$\underset{s}{med}(|log|\mathcal{W}f(s,x)| - log(A) - \alpha log(s)|^2).$$

Fig. 2 shows the wavelet transforms and the wavelet modulus maxima of a function obtained by using the wavelet $(1 + i\mathcal{H})\psi(x)$, where $\psi(x)$ is the second derivatives of a Gaussian function. Our function is constructed with isolated singularities shown in (a). From left to right: In the left neighborhood of the first singularity, the signal behaves like $O(|x|^{0.2})$, whereas in its right neighborhood, the signal behaves like $O(|x|^{0.6})$. The second singularity is a Dirac, whose Lipschitz exponent is -1. The Lipschitz exponent of the third singularity is 1.5, and the fourth is a step singularity. The complex-valued wavelet transform is shown in (b). In (c) are shown the maxima lines detected from (b). There are four lines: the first line is not a vertical line since the two sides of the corresponding singular point behave differently while the rest of the maxima lines are vertical. The real part of (b) is given in (d). In (e) are shown the maxima lines detected from (d). We observe that there are more maxima lines converging to each singular point in (e) than there are in (c) due to the oscillation of the real wavelet transform. There are three maxima lines in the first singularity. The left maxima line corresponds to the behavior of the left neighborhood of the singularity, which is $O(|x|^{0.2})$, the right maxima line corresponds to the behavior of the right neighborhood of the singularity, which is $O(|x|^{0.6})$, and the middle maxima line corresponds to the behavior of the singularity which is the compromise of the behaviors of the left and right neighborhoods at the singular point, with a behavior like $O(|x|^{0.3})$. In (f), we plot the decay of $log(|\mathcal{W}f(s,x)|)$ as a function of $log(s)$ along the maxima line of $|\mathcal{W}f(s,x)|$ of the first singularity. The maxima line of (c) is plotted with a solid line. The Lipschitz exponent of the line is 0.3, which is the

compromise the behaviors of the left and right neighborhoods of the singularity. There are three maxima lines corresponding to the first singularity in (d). The three maxima lines from left to right are plotted with '–', '-.', and '.', respectively. Their corresponding slopes are indicated on the lines.

3.2 Oscillating Singularities

In the previous section, we considered non-oscillating singularities; *i.e.*, satisfying $\forall x, f'(x)$ is Hölder $\alpha - 1$ iff $f(x)$ is Hölder α. Here, we will consider functions having singularities created by fast oscillations. For these functions, we will not have finite-deviations of their real and imaginary wavelet transforms of any interval containing the oscillating singularities. These singularities, therefore, can not be fully characterized by the theorems given in the previous section and their Hölder exponents. We give in the following a typical chirp function creating such singularities [3]

$$f(x) = |x - x_0|^h sin(\frac{1}{|x - x_0|^\beta}), \quad h, \beta > 0. \tag{10}$$

This function is singular at $x = x_0$, and its Hölder exponent is $h(x_0) = h$. However, the oscillating exponent β plays a very important role in the regularity of the primitive of $f(x)$. Indeed, one can show that the primitive of $f(x)$ is singular at $x = x_0$ with the Hölder exponent being $h + 1 + \beta$. Fig. 3(a) shows the chirp function with $h = 0.0$ and $\beta = 1$, where $f(x) = sin(\frac{1}{x^\beta})$, and shows that it is oscillating at $x = 0$. Fig. 3(b) shows the magnitude of the wavelet transform of (a) using the progressive wavelet $\Psi(x) = (1 + i\mathcal{H})\psi(x)$, where $\psi(x)$ is a real-valued wavelet.

Let $|\mathcal{W}f(s, x)|$ be the complex-valued wavelet modulus. The ridges at x_0 can be approximately obtained from the local maxima of $|\mathcal{W}f(s, x_0)|$ along s, with a fixed position at x_0. The following theorem states that the ridges of $|\mathcal{W}f(s, x)|$ form a continuous parabolic curve in the scale space (s, x).

Theorem 4 *If $f(x) = sin(\frac{1}{x^\beta})$, and if $\mathcal{W}f(s, x)$ is the wavelet transform of $f(x)$ using the wavelet $\Psi(x) = (1 + i\mathcal{H})\psi(x)$, where $\psi(x)$ is a real-valued wavelet, then*

in the scale space of $|\mathcal{W}f(s,x)|$*, there is continuous ridge that converges to* $(0,0)$*, and along this ridge* $s = Kx^{1+\beta}$*, where* K *is a constant.*

Proof:

$$\hat{\mathcal{W}f}(s,w) = \frac{\pi}{i}(\delta(\omega + \frac{\beta}{x^{\beta+1}}) - \delta(\omega - \frac{\beta}{x^{\beta+1}}))\hat{\Psi}(s\omega),$$

and since $\Psi(x)$ is a progressive wavelet, the negative frequency part vanishes. Therefore,

$$|\mathcal{W}f(s,x)| = \pi|\Psi(s\frac{\beta}{x^{\beta+1}})|.$$

Let K be the argument of $|\Psi(K)|$ such that $|\Psi(K)|$ is a maximum. Then, the ridges lie on a continuous curve in the scale space with $s\frac{\beta}{x^{\beta+1}} = K$. □

One can compare this result to that obtained by processing the same function by means of a real-valued spline wavelet in [13]. A general maxima is in the place along a maxima line where the maximal amplitude occurs. In [13], the parabolic function $s\frac{\beta}{x^{\beta+1}} = K$ was obtained by fitting the general maxima sampled from all the maxima lines. The general maxima of a real-valued wavelet transform form a discrete sampling of the parabolic function (see Fig. 3(d)) while in the complex-valued wavelet transform, the ridges form a continuous parabolic function (see Fig. 3(c)). The advantage of using the complex-valued wavelet transform in locating the oscillating singularity and in characterizing the oscillating exponent β is obvious.

4 Potential Applications

We will next present some potential applications of our methods. Our wavelet is a complex-valued progressive wavelet of the type $\Psi(x) = (1 + i\mathcal{H})\psi(x)$, where $\psi(x)$ is the Gaussian n-th derivative. In our experiments, we take $n = 2$.

4.1 Curvature Singularities Created by Spiral-Like Curves

Spiral curves have been investigated by many researchers since they exhibit beautiful symmetry in nature [19]. Let $\theta(t)$ be the argument, let $r(t)$ be the radius, and let $\kappa(t)$ be the curvature. We create spiral-like curves by controlling the relation between $r(t)$ and $\theta(t)$ such that $r(t) = \theta(t)^{-\frac{\beta}{\beta-1}}$, where β is a parameter. We will show that a curvature singularity is created at $t = 0$.
Let $s(t)$ be the length parameterized path following the contour of a spiral . We have assumed that $r(t)$ varies slower than $\theta(t)$ does. Then, we have

$$ds(t) = r(t)d\theta(t)$$

and, therefore,

$$ds(t)/dt = K(constant) = s'(t) = r(t)\theta'(t). \tag{11}$$

We can substitute

$$r(t) = \theta(t)^{-\frac{\beta}{\beta-1}}$$

into Equation (11) and by means of simple calculations, we have

$$\begin{aligned}
K_1 &= \theta'(t)r(t) = \kappa(t)\theta(t)^{-\frac{\beta}{\beta-1}} \quad , \quad \text{where } K_1 \text{ is a constant;} \\
\theta(t) &= \frac{K_2}{\kappa(t)^{1-\beta}\beta} \quad , \quad \text{where } K_2 \text{ is a constant;} \\
\theta'(t) &= \kappa(t) = K_1\frac{\beta-1}{\beta}\kappa(t)^{\frac{-1}{\beta}}\kappa'(t); \\
\kappa(t)^{\frac{\beta+1}{\beta}} &= K_3\kappa'(t), \quad \text{where } K_3 \text{ is a constant.}
\end{aligned} \tag{12}$$

The solution of Equation(12) for curvature is

$$\kappa(t) = ct^{-\beta}, \quad \text{where } c \text{ is a constant;}$$

therefore, the argument is

$$\theta(t) = d \cdot t^{-\beta+1} + e, \quad \text{where } d \text{ and } c \text{ are constants.}$$

In Figs. 4(a) and (b), the spiral-like curves are created by $r(\theta) = a*(\theta)^{\frac{\beta}{1-\beta}}+c$ with $\beta = 0.4$ in (a) and $\beta = 0.8$ in (b), respectively. We traced the curves inwards first,

so the curvature is increasing, and then we traced backwards, so the curvature is decreasing, to the outside. A chain-code representation was created as our traced along the curve [5]. The Lipschitz exponent in (a) is $0.594 \approx 1 - 0.4$, and that in (b) is $0.212 \approx 1 - 0.8$. In (c) and (d), we show the decay of $log_2|\mathcal{W}\theta(s,x)|$ as a function of $log_2(s)$ along the maxima line at the singular points of (a) and (b), respectively.

4.2 Contour Segmentation

The contour of a planar shape is very useful for recognizing the planar shape [4][17]. It can be represented by means of chain codes. For recognition purposes, a contour is usually segmented into components. A typical approach is to locate the salient points, usually corresponding to curvature singularities, along the contour and to then segment the contour using them. However, not all the salient points are suitable for segmentation purposes. An example is the salient points in the fin of a fish. Although there are many curvature singular points in the fin, we would not use them to segment the fish. Doing so would cut the fin into pieces. Instead, these points are better regarded as a coherent piece.

In the Introduction, we mentioned that one is able to extract instantaneous frequencies from the modulus of a complex-valued wavelet transform. In this article, we have shown that the wavelet modulus maxima of a complex-valued wavelet can be used to detect and characterize singularities. Thus, we are able to detect simultaneously instantaneous frequencies and singularities from the wavelet modulus maxima of a complex-valued wavelet. Thus, when the contour of a shape is composed of frequency components and isolated singular points, we can use the modulus maxima of a complex-valued wavelet to detect both. After some proper deletion of unwanted ridges or wavelet modulus maxima, the contour of a shape is then divided into sub-contours of frequency components and smooth curves.

We use the following method to distinguish those sub-contours which are dominated by frequency components from those by smooth curves: We compute both the modulus maxima and ridge of the wavelet transform. First, we remove the maxima lines which are too short or which have Lipschitz exponents not in

the interest region. Then, we chain the ridges horizontally along the position x by assuming that the ridges form a smooth curve in the wavelet transform modulus . Then, we remove those ridges whose lengths are too short based on a threshold whose values are proportional to the length of the contour. The remaining ridges are regarded as covering the parts of the contour dominated by the frequency variations. We then remove all the modulus maxima within those sub-contours which are dominated by frequency information. At this point, we have partitioned the contour into components according to the modulus maxima. The sub-contour within two adjacent modulus maxima contains either a frequency dominant region or no frequency region.

Fig. 5 presents an example of applications of our segmentation algorithm to a fish. From the chain-code of the fish, we computed its wavelet transform by taking the complex-valued progressive wavelet $\Psi(x) = (1 + i\mathcal{H})\psi(x)$, where $\psi(x)$ is the second derivative of a Gaussian function. The wavelet modulus maxima and ridges were, then, computed from the modulus of the wavelet transform, respectively. The maxima lines (in (a)) and the ridge curves (in (b)) were obtained by connecting the neighboring modulus maxima and the ridges, respectively. Then, we deleted the maxima lines that were too short or whose corresponding Lipschitz exponents were not of interests (in (c)). In (d), we show the remaining ridge curves we obtained after deleting the ridge curves which were too short. As shown in (f), we superimposed the singular points from modulus maxima lines in (a) onto the boundary of the fish. In (g), the singular points from the maxima lines in (d) are superimposed to the fish. The contour of the fish was divided into subcomponents with frequencies and with smooth curves divided by salient points. This segmentation algorithm can potentially be used in planar shapes recognition. We are currently investigating this problem.

5 Conclusion

We have proved that the wavelet transform modulus maxima of a complex-valued wavelet can detect and characterize the singularities of a real-valued func-

tion. We have also shown that the ridges of a complex-valued wavelet transform provide a better representation than do the general maxima of a real-valued wavelet transform for locating oscillating singularities and characterizing the oscillating exponents. We have presented some potential applications of our methods in characterization of curvature singularities and in segmentation of the contours of planar shapes.

Acknowledgment Wen-Liang Hwang would like to express his gratitude to Professors S. Mallat, B. Torrésani, and E. Bacry. They have taught him a lot about modulus maxima and ridges.

Appendix A

In this appendix, we review a well-known theorem, a proof of which can be found in [10][15].

Theorem 5 *: Let $f(x)$ be a real-valued function, and let $[a, b]$ be an interval of R. Let $0 < \alpha < 1$. Then, $f(x)$ is uniformly Lipschitz α over $(a+\epsilon, b-\epsilon)$, if and only if for any $\epsilon > 0$, there exists a constant A_ϵ such that for all $x \in (a+\epsilon, b-\epsilon)$ and $s > 0$, $|\mathcal{W}f(s,x)| \leq A_\epsilon s^\alpha$.*

One can easily show that the abovementioned theorem is also true for a complex-valued wavelet $\Psi(x) = \Psi_R(x) + i\Psi_I(x)$, provided that $\Psi_R(x)$, $\Psi_I(x)$, $\frac{d\Psi_R(x)}{dx}$, and $\frac{d\Psi_I(x)}{dx}$ are all in $L^1(R)$. The abovementioned theorem can be extended to a Lipschitz exponent α larger than 1 by imposing the wavelet has enough vanishing moments. One can find related discussion in [13].

Appendix B

We need the following lemmas for our Theorem 2.

Lemma 1 *Let $f(x)$ be a real-valued function. If* $\forall x \in [t_0, t_1], \quad |f'(x)| > C > 0$, *then* $\int_{t_0}^{t_1} |f(x)|dx > \frac{1}{4}(t_1 - t_0)^2 C$.

Proof:

Since $|f'(x)| > C > 0$, we know that $f'(x)$ is a function with a constant sign in $[t_0, t_1]$. For simplicity, we will only discuss the case where $f'(x)$ are all positive in $[t_0, t_1]$. Since $f'(x)$ are all positive , $f(x)$ is strictly monotonically increasing in $[t_0, t_1]$. We will present our result by discussing the following two cases :

Case1 : $f(x)$ intersects with the x axis

Suppose $f(t) = 0$, $t \in [t_0, t_1]$. Since $\int_t^x f'(x)dx = f(x)$, we have $f(x) > C(x - t)$. Therefore, $\int_t^{t_1} f(x)dx > \frac{1}{2}C(t_1 - t)^2$. By a similar argument, we have $-\int_{t_0}^{t} f(x)dx > \frac{1}{2}C(t - t_0)^2$. Then,

$\int_{t_0}^{t_1} |f(x)|dx > \frac{1}{2}((t - t_0)^2 C + (t_1 - t)^2 C) \geqq \frac{1}{4}C(t_1 - t_0)^2$.

Case2 : $f(x)$ does not intersect with the x axis

Suppose $f(x) > 0$, for $x \in [t_0, t_1]$. Since $f(x) - f(t_0) = \int_{t_0}^x f'(x)dx > C(x - t_0)$, we have $\int_{t_0}^{t_1} f(x)dx > \int_{t_0}^{t_1} f(x)dx - f(t_0)(t_1 - t_0) > \frac{1}{2}C(t_1 - t_0)^2$.

Similarly, let $f(x) < 0$ for $x \in [t_0, t_1]$. Since $f(t_1) - f(x) = \int_x^{t_1} f'(x)dx < C(t_1 - x)$, we have $-\int_{t_0}^{t_1} f(x)dx > -\int_{t_0}^{t_1} f(x)dx + f(t_1)(t_1 - t_0) > \frac{1}{2}C(t_1 - t_0)^2$.

Based on cases 1 and 2, we, have

$\int_{t_0}^{t_1} |f(x)|dx > \frac{1}{4}(t_1 - t_0)^2 C$. $\square$

Lemma 2 *Let $f(x)$ be a real-valued function. If* $\forall x \in [t_0, t_1], \quad |f''(x)| > C > 0$, *then* $\int_{t_0}^{t_1} |f(x)|dx > \frac{1}{16}(\frac{t_1 - t_0}{3})^3 C$.

Proof:

Since $f''(x)$ is a constant sign function in $[t_0, t_1]$, $f'(x)$ is strictly monotonically increasing or decreasing function in $[t_0, t_1]$. We have :

$(\frac{t_1 - t_0}{3}) max(|f'(t_0 + \frac{1}{3}(t_1 - t_0))|, |f'(t_0 + \frac{2}{3}(t_1 - t_0))|) \geqq \int_{t_0 + \frac{1}{3}(t_1 - t_0)}^{t_0 + \frac{2}{3}(t_1 - t_0)} |f'(x)|dx > \frac{1}{4}(\frac{t_1 - t_0}{3})^2 C$. The last inequality in the above follows from Lemma 1.

Without loss of generality, let us suppose that $max(|f'(t_0 + \frac{1}{3}(t_1 - t_0))|, |f'(t_0 + \frac{2}{3}(t_1 - t_0))|) = |f'(t_0 + \frac{2}{3}(t_1 - t_0))|$. Then, $f'(x)$ must be either all positive values or

all negative values within the interval $[t_0+\frac{2}{3}(t_1-t_0), t_1]$. If this is not the case, then $|f'(t_0+\frac{1}{3}(t_1-t_0))| > |f'(t_0+\frac{2}{3}(t_1-t_0))|$, and a violation of our assumption occurs. Thus, we have for any $x \in [t_0+\frac{2}{3}(t_1-t_0), t_1]$: $|f'(x)| > |f'(t_0+\frac{2}{3}(t_1-t_0))| > 0$. By Lemma 1,

$\int_{t_0+\frac{2}{3}(t_1-t_0)}^{t_1} |f(x)|dx > \frac{1}{4}(\frac{t_1-t_0}{3})^2 |f'(t_0+\frac{2}{3}(t_1-t_0))| \geq \frac{1}{4}(\frac{t_1-t_0}{3})^3 \frac{1}{4}C = \frac{1}{16}(\frac{t_1-t_0}{3})^3 C$.
Therefore, $\int_{t_0}^{t_1} |f(x)|dx > \int_{t_0+\frac{2}{3}(t_1-t_0)}^{t_1} |f(x)|dx > \frac{1}{16}(\frac{t_1-t_0}{3})^3 C$. $\square$

Lemma 3 *Let K be a positive constant. Let $g(x)$ be a complex function which satisfies $\int_c^d |g(x)|dx < K$. Suppose that $|\frac{dg(x)}{dx}|$ has no local maxima in $[c,d]$. Let $\beta > 0$, and let the first derivatives of $Re(g(x))$ and $Im(g(x))$ be finite-deviations; then, there exists a constant C_β such that for all x in $[c+\beta, d-\beta]$, $|\frac{dg(x)}{dx}| < C_\beta$.*

Proof:

Since $|g'(x)|$ has no local maxima in $[c,d]$, for all x in $[c+\beta, d-\beta]$, $|g'(x)| < max(|g'(c+\beta)|, |g'(d-\beta)|)$. Without loss of generality, let us suppose that $max(|g'(c+\beta)|, |g'(d-\beta)|) = g'(c+\beta)$. Then, for all x in $[c, c+\beta]$, $|g'(x)| > |g'(c+\beta)| > 0$. By Lemma 1, we have $\int_{c+\frac{\beta}{2}}^{c+\beta} |g(x)|dx > \frac{1}{4}(c+\beta-c-\frac{\beta}{2})^2 |g'(c+\beta)|$. Since $\int_c^d |g(x)|dx < K$, we then have $K > \int_c^d |g(x)|dx > \int_{c+\frac{\beta}{2}}^{c+\beta} |g(x)|dx > \frac{1}{4}(c+\beta-c-\frac{\beta}{2})^2 |g'(c+\beta)|$; therefore, for all x in $[c+\beta, d-\beta]$, $|g'(x)| < |g'(c+\beta)| < \frac{16K}{\beta^2}$.

Let $g(x) = a(x) + ib(x)$, where $a(x) = Re(g(x))$ and $b(x) = Im(g(x))$ are real functions. Since the first derivatives of $Re(g(x))$ and $Im(g(x))$ are finite-deviation, we can divide the interval $[c+\frac{\beta}{2}, c+\beta]$ into $M(\beta)$ subintervals $v_1, v_2, ..., v_M$ with, in each interval v_i, either $a'(x) = b'(x)$ for all x in v_i or $a'(x) = b'(x)$ only at the two ends of the subinterval v_i.

We now define a real function $c(x)$ over $[c+\frac{\beta}{2}, c+\beta]$ such that

$$c(x) = \begin{cases} a(x) & if |a'(x)| \geq |b'(x)|, \\ b(x) & if |b'(x)| > |a'(x)|. \end{cases}$$

As a result, we have $|c'(x)| \geq \frac{|g'(x)|}{\sqrt{2}} > \frac{|g'(c+\beta)|}{\sqrt{2}} > 0$ for $x \in [c+\frac{\beta}{2}, c+\beta]$. We can now apply Lemma 1 to each interval $v_i, i = 1, 2, ..., M(\beta)$ over $[c+\frac{\beta}{2}, c+\beta]$ and obtain $\int_{v_i} |c(x)|dx > \frac{1}{4}|v_i|^2 \frac{|g'(c+\beta)|}{\sqrt{2}}$, where $|v_i|$ is the length of the subinterval v_i.

Furthermore, we have

$$K > \int_c^d |g(x)|dx > \int_{c+\frac{\beta}{2}}^{c+\beta} |c(x)|dx = \sum_i \int_{v_i} |c(x)|dx > \sum_i |v_i|^2 \frac{|g'(c+\beta)|}{4\sqrt{2}}. \quad (13)$$

It is not hard to show that $(\sum_i |v_i|^2)M(\beta) \geqq (\sum_i |v_i|)^2 = \frac{\beta^2}{4}$. Therefore, $\sum_i |v_i|^2 \geqq \frac{\beta^2}{4M(\beta)}$. Substituting this into the equation (13), we have $K > \frac{1}{4\sqrt{2}} \frac{\beta^2}{4M(\beta)} |g'(c+\beta)|$ and, therefore, $|g'(c+\beta)| < \frac{16\sqrt{2}M(\beta)K}{\beta^2} = C_\beta$. As a result, for all x in $[c+\beta, d-\beta]$, $|g'(x)| < C_\beta$. $\square$

Lemma 4 *Let K be a positive constant, and let $g(x)$ be a complex-valued function which satisfies*

$$\int_c^d |g(x)|dx < K.$$

Suppose that $|\frac{d^2 g(x)}{dx^2}|$ has no local maxima in $[c,d]$. Let $\beta > 0$, and let the second derivatives of $Re(g(x))$ and $Im(g(x))$ be finite-deviations; then, there exists a constant D_β such that for all x in $[c+\beta, d-\beta]$, $|\frac{d^2 g(x)}{dx^2}| < D_\beta$.

Proof:

The proof of this lemma is similar to that of the previous lemma.

$|g''(x)|$ has no local maxima for all x in $[c,d]$. Then, for all x in $(c+\beta, d-\beta)$, $|g''(x)| \leqq max(|g''(c+\beta)|, |g''(d-\beta)|)$. Without loss of generality, let us suppose that $max(|g''(c+\beta)|, |g''(d-\beta)|)$ is equal to $|g''(c+\beta)|$. Then, for $x \in [c+\frac{\beta}{2}, c+\beta]$, we have $|g''(x)| > |g''(c+\beta)| > 0$. By Lemma 2, we have $K > \int_c^d |g(x)|dx > \int_{c+\frac{\beta}{2}}^{c+\beta} |g(x)|dx > \frac{1}{16}(\frac{c+\beta-c-\frac{\beta}{2}}{3})^3 |g''(c+\beta)|$. Therefore, for all x in $[c+\beta, d-\beta]$, $|g''(x)| < |g''(c+\beta)| < \frac{384K}{\beta^3}$.

Let $g(x) = a(x) + ib(x)$, where $a(x) = Re(g(x))$ and $b(x) = Im(g(x))$ are real functions. Since the second derivatives of $Re(g(x))$ and $Im(g(x))$ are finite-deviations, we can divide $[c+\frac{\beta}{2}, c+\beta]$ into $M(\beta)$ subintervals $v_1, v_2, ..., v_M$, with in each subinterval v_i, either $a''(x) = b''(x)$ for all x in the subinterval or $a''(x) = b''(x)$ only at the two ends of the subinterval. Let a real function $c(x)$ be

$$c(x) = \begin{cases} a(x) & if |a''(x)| \geq |b''(x)|, \\ b(x) & if |b''(x)| > |a''(x)|. \end{cases}$$

Then, we have $|c''(x)| \geqq \frac{|g''(x)|}{\sqrt{2}} > \frac{|g''(c+\beta)|}{\sqrt{2}} > 0$ for $x \in [c+\frac{\beta}{2}, c+\beta]$. For a subinterval v_i, by Lemma 2, we have $\int_{v_i} |c(x)|dx > \frac{1}{16}(\frac{|v_i|}{3})^3 \frac{|g''(c+\beta)|}{\sqrt{2}}$. Furthermore, we have

$$K > \int_c^d |g(x)|dx > \int_{c+\frac{\beta}{2}}^{c+\beta} |c(x)|dx = \sum_i \int_{v_i} |c(x)|dx > \sum_i \frac{1}{16}(\frac{|v_i|}{3})^3 \frac{|g''(c+\beta)|}{\sqrt{2}}. \quad (14)$$

Assume that $\beta < 1$. Then, all $|v_i| < 1$ and ,therefore, $\sum_i |v_i|^3 \geqq \sum_i |v_i|^4$. It is not hard to show that $\sum_i |v_i|^4 \geqq \frac{(\sum_i |v_i|^2)^2}{M(\beta)}$. Then, we have $\sum_i |v_i|^3 \geqq \sum_i |v_i|^4 \geqq \frac{(\sum_i |v_i|^2)^2}{M(\beta)} \geqq \frac{\beta^4}{16(M(\beta))^2}$. Substituting this into the equation (14), we then have $K > \frac{1}{16}\frac{1}{3^3}\frac{\beta^4}{16(M(\beta))^2}\frac{|g''(c+\beta)|}{\sqrt{2}}$. Then, we have $|g''(c+\beta)| < \frac{2^8 3^3 \sqrt{2}(M(\beta))^2 K}{\beta^2} = D_\beta$. Thus, we have for all x in $[c+\beta, d-\beta]$, $|g''(x)| < D_\beta$. $\square$

Appendix C

PROOF OF THEOREM 2

We will prove this theorem by induction with the following proposition.

Proposition(P_n) :

Let $\Psi(x)$ be a complex-valued wavelet that can be written as $\Psi(x) = d^n\Phi(x)/dx^n$. $\Phi(x)$ is equal to $\Phi_R(x) + i\Phi_I(x)$, and both $\Phi_R(x)$ and $\Phi_I(x)$ are continuous functions of compact support. Let $f(x)$ be a real function. Then, for any $\epsilon > 0$, there exists a constant K_ϵ such that at all scales s,

$$\int_{a+\epsilon}^{b-\epsilon} |f * \Phi_s(x)|dx \leq K_\epsilon, \tag{15}$$

where $\Phi_s(x) = \frac{1}{s}\Phi(\frac{x}{s})$.

If $\mathcal{W}f(s,x)$ has no maxima for $x \in (a,b)$ and $s < s_0$, then for any $\epsilon > 0$, there exists a constant $A_{\epsilon,n}$ such that for any $x \in (a+\epsilon, b-\epsilon)$ and $s < s_0$,

$$|\mathcal{W}f(s,x)| \leq A_{\epsilon,n}s^n. \tag{16}$$

If we modify $f(x)$ by multiplying it by the indicator function of $[a,b]$, we will not modify its regularity on any interval $[a+\epsilon, b-\epsilon]$. In the following, we shall, thus, assume that $f(x) = 0$ for all $x \notin [a,b]$.

Let us first prove that (15) is satisfied:

Since $f(x) \in L^1([a,b])$ and $f(x) = 0$ for all $x \notin [a,b]$, it follows that

$$\int_a^b |f * \Phi_s(x)|dx \leq \int_a^b |f(x)|dx \int_{-\infty}^{+\infty} |\Phi_s(x)|dx.$$

With a change of variable in the integral, we obtain

$$\begin{aligned} \int_{-\infty}^{+\infty} |\Phi_s(x)|dx &= \int_{-\infty}^{+\infty} |\Phi(x)|dx \\ &\leq \int_{-\infty}^{+\infty} |\Phi_R(x)|dx + \int_{-\infty}^{+\infty} |\Phi_I(x)|dx. \end{aligned}$$

Hence, $\int_a^b |f * \Phi_s(x)|dx$ is bounded by a constant independent of the scales, as in (15).

Let us now prove that (16) is satisfied:

We will first prove that the proposition is true for $n = 1$. Since $\Psi(x) = d\Phi(x)/dx$, we find that

$$\mathcal{W}f(s,x) = s\frac{d}{dx}(f * \Phi_s)(x).$$

Let $g(x) = (f * \Phi_s)(x)$. By (15) and Lemma 3, we have for all $x \in [c+\epsilon, d-\epsilon]$, $|\frac{d}{dx}(f * \Phi_s)(x)| < A_{\epsilon,1}$. Therefore, $|\mathcal{W}f(s,x)| \leq sA_{\epsilon,1}$.

The proof of (P_n) for $n = 2$ is based on (15) and Lemma 4. Since $\Psi(x) = d^2\Phi(x)/dx^2$, we find that

$$\mathcal{W}f(s,x) = s^2\frac{d^2}{dx^2}(f * \Phi_s)(x).$$

For all $x \in [c+\epsilon, d-\epsilon]$, $|\frac{d^2}{dx^2}(f * \Phi_s)(x)| < A_{\epsilon,2}$. Therefore, $|\mathcal{W}f(s,x)| \leq s^2 A_{\epsilon,2}$.

Let us now prove that if (P_n) is true, for $n \geq 2$, then (P_{n+1}) is also true. Let $\Psi(x)$ be a wavelet with $n+1$ vanishing moments. The wavelet $\Psi(x)$ can be written $\Psi(x) = d\chi(x)/dx$ where $\chi(x)$ is a wavelet that has n vanishing moments. Let $df(x)/dx$ be the derivative of $f(x)$ in the sense of distributions; then,

$$\mathcal{W}f(s,x) = s\frac{df}{dx} * \chi_s(x). \tag{17}$$

In order to apply our induction hypothesis (P_n) to $df(x)/dx$ with respect to the wavelet $\chi(x)$, we need to prove for any $\epsilon > 0$ that there exists a constant K_ϵ such that at all scales s,

$$\int_{a+\epsilon}^{b-\epsilon} |\frac{df}{dx} * \Phi_s(x)|dx \leq K_\epsilon. \tag{18}$$

Since the wavelet $\Psi(x)$ has more than rwo vanishing moments, the proposition (P_2), which we just proved, implies that for any $\epsilon > 0$, if $x \in (a+\epsilon, b-\epsilon)$,

$$|\mathcal{W}f(s,x)| \leq s^2 A_{\epsilon,2}.$$

From Theorem 5 (in Appendix A), we find that $f(x)$ is uniformly Lipschitz α on the intervals $(a+\epsilon, b-\epsilon)$, for any $\alpha < 2$. Hence, $df(x)/dx$ is uniformly bounded on any such interval. We can then easily derive that (18) is satisfied.

Let us now apply the induction hypothesis (P_n) to $df(x)/dx$ with respect to the wavelet $\chi(x)$. There exists a constant $A_{\epsilon,n}$ such that for any $x \in (a+\epsilon, b-\epsilon)$ and $s < s_0$,

$$|\frac{df}{dx} * \chi_s(x)| \leq A_{\epsilon,n} s^n.$$

Equation (17) implies that

$$|\mathcal{W}f(s,x)| \leq A_{\epsilon,n} s^{n+1}.$$

This finishes the proof of (P_{n+1}).

By applying Theorem 5 (in Appendix A) to the statement (P_n), we derive that the function $f(x)$ is Lipschitz α for any $\alpha < n$.

Let us now prove that (16) implies that $f(x)$ is Lipschitz n if the wavelet $\Psi(x)$ can be written as

$$\Psi(x) = \frac{d^n \theta(x)}{dx}, \tag{19}$$

where $\theta(x) = \theta_R(x) + i\theta_I(x)$ and both $\theta_R(x)$ and $\theta_I(x)$ are smoothing functions. Let $d^n f(x)/dx^n$ be the n-th derivative of $f(x)$ in the sense of distributions. Similar to (17), (19) yields

$$\mathcal{W}f(s,x) = s^n \frac{d^n f}{dx^n} * \theta_s(x).$$

Equation (16) of proposition (P_n) implies that for any $\epsilon > 0$, there exists a constant $A_{\epsilon,n}$ such that for any $x \in (a+\epsilon, b-\epsilon)$ and $s < s_0$,

$$\begin{aligned} |\frac{d^n f}{dx^n} * \theta_s(x)| &\leq |\frac{d^n f}{dx^n} * (\theta_R)_s(x))| + |\frac{d^n f}{dx^n} * (\theta_I)_s(x))| \\ &\leq (A_R)_{\epsilon,n} + (A_I)_{\epsilon,n} \\ &\leq A_{\epsilon,n}. \end{aligned}$$

Since the integral of $\theta(x)$ is nonzero, this equation implies that $d^n f(x)/dx^n$ is a function that is bounded by $A_{\epsilon,n}$ over the interval $(a+\epsilon, b-\epsilon)$. Hence, $f(x)$ is uniformly Lipschitz n over the interval $(a+\epsilon, b-\epsilon)$. $\square$

Appendix D

PROOF OF THEOREM 3

First, we derive that that $f(x)$ is Lipschitz n at any $x \neq x_0$. For any $\epsilon > 0$, there exists a scale s_ϵ such that for all $s < s_\epsilon$, there is no wavelet modulus maxima at $(a + \epsilon, x_0 - \epsilon)$. Furthermore, since the n-th derivatives of $Re(\mathcal{W}f(s,x))$ and $Im(\mathcal{W}f(s,x))$ are finite-deviations for all s, from Theorem 2, the Lipschitz in the neighborhood of any $x_1 \in (a + \epsilon, x_0 - \epsilon)$ is n. Thus, $f(x)$ is uniform Lipschitz n at any point in (a, x_0). The same is true for any point in (x_0, b).

Let us prove that $f(x)$ is Lipschitz α at x_0 and can be characterized by the complex-valued wavelet modulus maxima. For any interval $(x_0 - \epsilon, x_0 + \epsilon)$ including x_0, there is a small enough scale s_ϵ such that for all $s < s_\epsilon$, the wavelet modulus maxima for these scales are contained entirely within the region $(x_0 - \epsilon, x_0 + \epsilon)$ by $(0, s_\epsilon)$. Then, there is a constant D_ϵ such that all the wavelet transform in the region will be bounded by

$$|\mathcal{W}f(s,x)| < D_\epsilon s^\alpha.$$

From Theorem 5, any subinterval including x_0 in $(x_0 - \epsilon, x_0 + \epsilon)$ will be Lipschitz α. This implies that the Lipschitz at x_0 is α.

References

[1] J. P. Antoine, R. Murenzi, "Two-dimensional directional wavelets and the scale-angle representation," *Signal Processing.*, 52, pp. 259-281, 1996.

[2] A. Arneodo, E. Bacry, S.Jaffard and J.F. Muzy, "The thermodynamics of fractals revisited with wavelets," *Physica A*, 213 (1995) 232-275.

[3] A. Arneodo, E. Bacry, S.Jaffard and J.F. Muzy, "Oscillating Singularities on Cantor Sets: A Grand-Canonical Multifractal Formalism," *Journal of Statistical Physics*, vol. 87, nos. 1/2, pp. 179-209, 1997.

[4] H. Asada and M. Brady, "The Curvature Primal Sketch," *IEEE Trans. Pattern Anal. Mach. Intell.*, 8(1), pp 2-14, 1986.

[5] D. H. Ballard and C. M. Brown, "Computer Vision," *Prentice Hall*, 1982.

[6] R. Carmona, W. L. Hwang, B. Torrésani, "Multiridge Detection and Time-Frequency Reconstruction," *IEEE Trans. on Signal Processing*, vol. 47, no. 2, February 1999.

[7] N. Delprat, B. Escudië, P. Guillemain, R. Kronland-Martinet, Ph. Tchamitchian, and B. Torrésani, "Asymptotic Wavelet and Gabor Analysis: Extraction of Instataneous Frequencies," *IEEE Trans. on Information Theorem*, vol. 38, no. 2, March 1992.

[8] H. Führ, W. L. Hwang, and B. Torrésani, "Shape from Texture using Continuous Wavelet Transform," *Accepted to be published in SPIE conference,* 2000.

[9] A. Grossmann and J. Morlet, "Decomposition of Hardy functions into square integrable wavelets of constant shape," *SIAM J. Math.*, vol. 15, pp. 723-736, 1984.

[10] M. Holschneider and Ph. Tchamitchian, "Regularite locale de la fonction non-differentiable de Riemann," *Lecture notes in Mathematics, P. G. Lemarie, Ed. New York*, Springer-Verlag, 1989.

[11] W. L. Hwang, C. S. Lu, and P. C. Chung, "Shape from Texture: Direct Estimation of Planar Surface Orientations Through the Ridge Surfaces of Continuous Wavelet Transform," *IEEE Transactions on Image Processing.*, vol. 7, no. 5, pp. 773-780, 1998.

[12] S. Mallat and S. Zhong, "Characterization of Signals from Multiscale Edges," *IEEE Trans. on Pattern Anal. Mach. Intell.*, vol. 14(7):710-732, July 1992.

[13] S. Mallat and W. L. Hwang, "Singularity Detection and Processing with Wavelets," *IEEE Trans. on Information Theory*, vol. 38, no. 2, pp. 617-643, March 1992.

[14] D. Mar, "Vision," *W. H. Freeman*, 1982.

[15] S. Jaffard, "Pointwise Smoothness, Two-Microlocalization and Wavelet Coefficients," *Publiicacions Matemátiques,* 35:155-168, 1991.

[16] S. Jaffard, "Multifractal formalism ofr functions parts I and II," *SIAM J. of Mathematical Analysis,* 1997.

[17] F. Mokhtarian, A. Mackworth, "A Theory of Multiscale, Curvature-based Shape Representation for Planar Curves," *IEEE Trans. Pattern Anal. Mach. Intell.*, 14, pp 789-805, 1992.

[18] J. M. Steele, W. L. Steiger, "Algorithm and Complexity for Least Median of Squares Regression," *Discrete Applied Mathematics*, 14, pp 93-100, 1986.

[19] H. Weyl, "Symmetry," *Princeton University Press*, 1989.

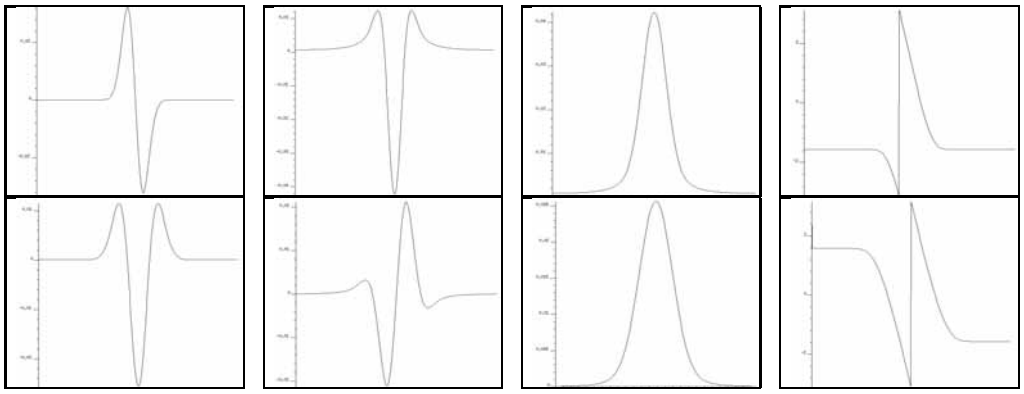

(a) (b) (c) (d)

Figure 1: Complex-valued wavelet with type $(1+i\mathcal{H})\psi_n(x)$, where $\psi_n(x)$ is defined in Eq. (5). We show the cases $n = 1$(top) and $n = 2$(bottom) with the (a) real part, (b) imaginary part, (c) amplitude, and (d) phase.

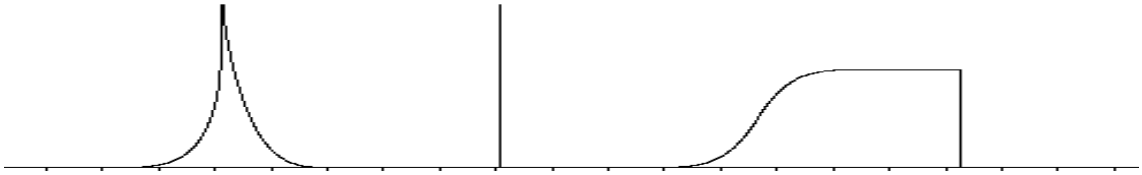

(a)

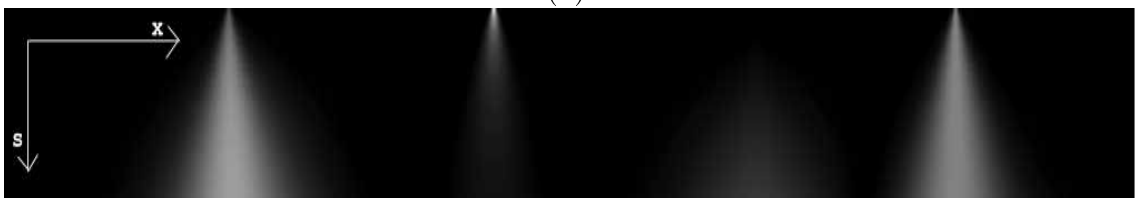

(b)

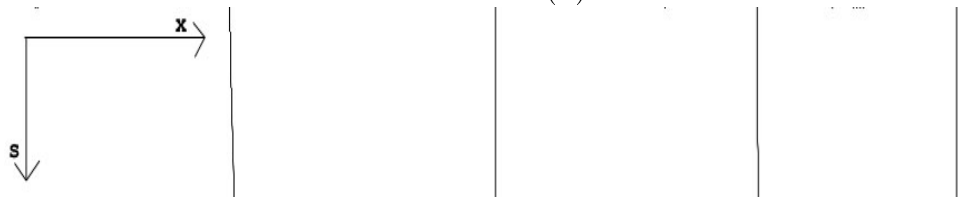

(c)

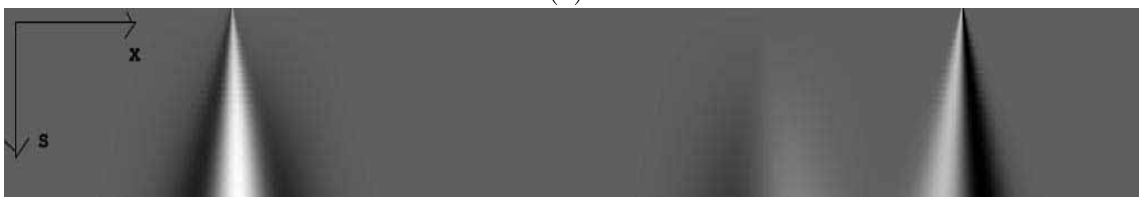

(d)

(e)

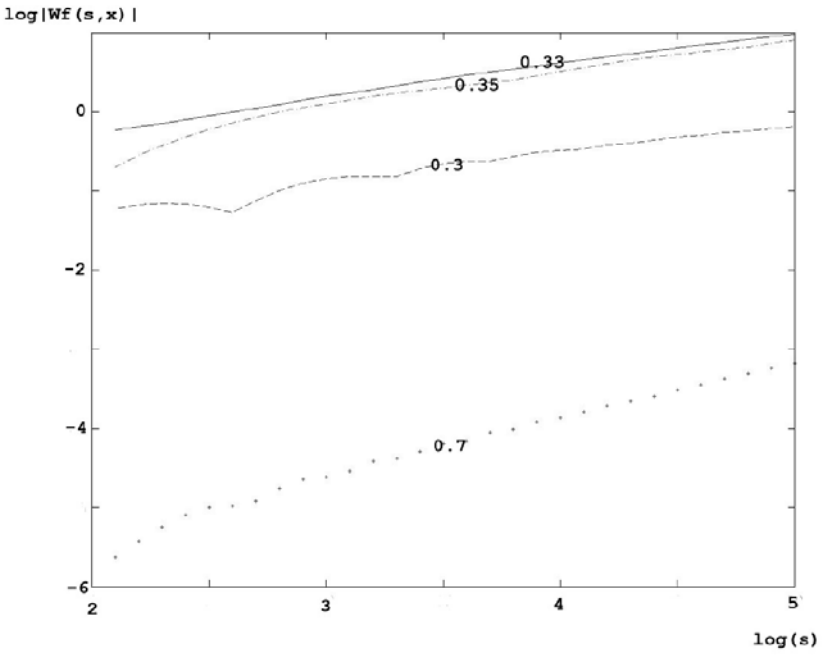

(f)

Figure 2: (a) There are four singularities from left to right in this signal. In the left neighborhood of the first singularity, the signal locally behaves like $O(|x|^{0.2})$, whereas in its right neighborhood, the signal behaves like $O(|x|^{0.6})$. The second singularity is a Dirac whose Lipschitz is -1. The Lipschitz exponent of the third singularity is 1.5. The fourth is a step singularity. (b) The complex-valued wavelet transform of (a). (c) The maxima line of (b). (d) The real part of the wavelet transform in (b). (e) The maxima lines of (d), in which there are three maxima lines corresponding to the first singularity. The left maxima line corresponds to the left neighborhood of the singularity with $O(|x|^{0.2})$, and the right maxima line corresponds to the right neighborhood of the singularity with $O(|x|^{0.6})$. The middle maxima line is the compromise behavior between the left and right neighborhoods of the singularity. (f) Decay of $log(|\mathcal{W}f(s,x)|)$ as a function of $log(s)$ along the maxima lines of the first singularity. The maxima line of (c) is plotted with a solid line. The three maxima lines of (e) from left to right of are plotted with '–', '-.', and '.'. Their slopes are recorded on the lines.

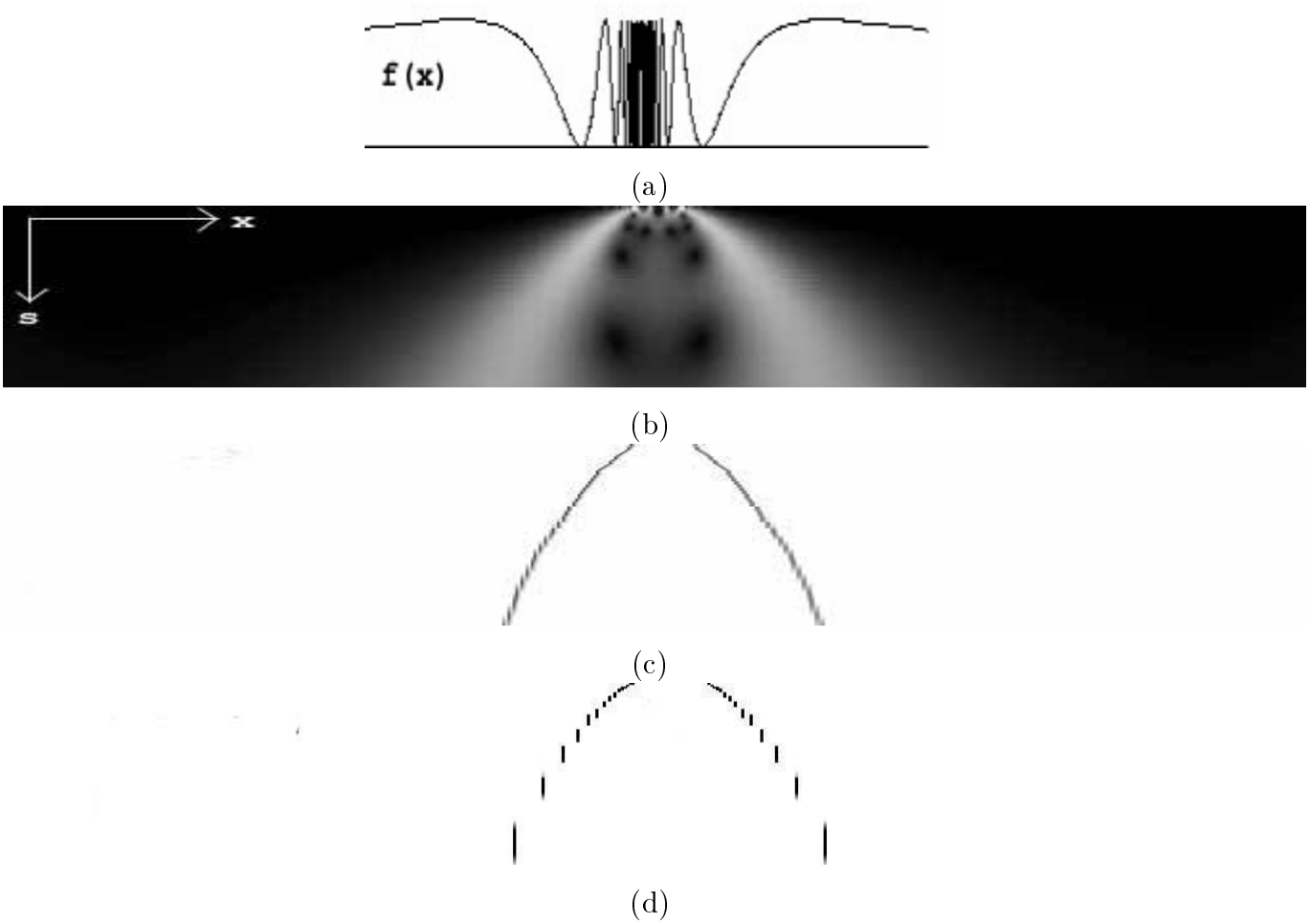

Figure 3: Oscillating singularity. (a) The chirp function with $h = 0$ and $\beta = 1$. (b) The wavelet transform magnitude obtained using a complex-valued wavlet with the chirp function of (a). (c) The ridges of the wavelet transform, which is a continuous curve. (d) General maxima obtained from the real part of the wavelet transform. These are discrete samplings of the continuous parabolic function at (c). We have enlarged the blach dot for easier visibility.

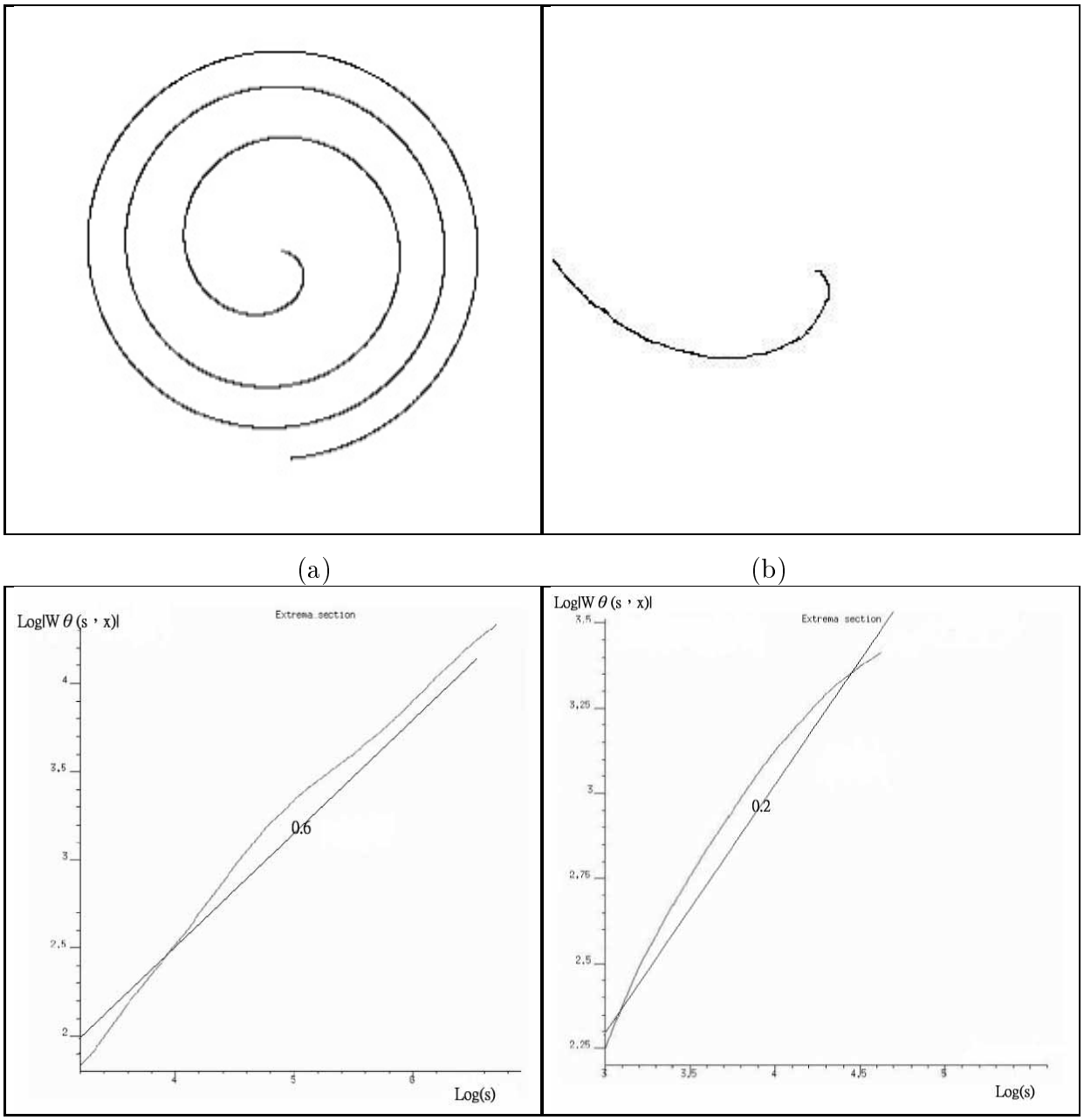

Figure 4: (a) (b) Spiral-like curves with chain code function $\theta(x) = \frac{x^{1-\beta}}{1-\beta}$. In (a), β is 0.4, and in (b), β is 0.8. (c) (d) Decay of $\log|\mathcal{W}f(s,x)|$ as a function of $\log(s)$ along the maxima line at the singular points of (a) and (b); The singular point is created by tracing the contours of (a) and (b) inwards first and, then tracing outwards. The lines were computed by fitting the least median squares to the sampled data. The slopes are recorded on the lines.

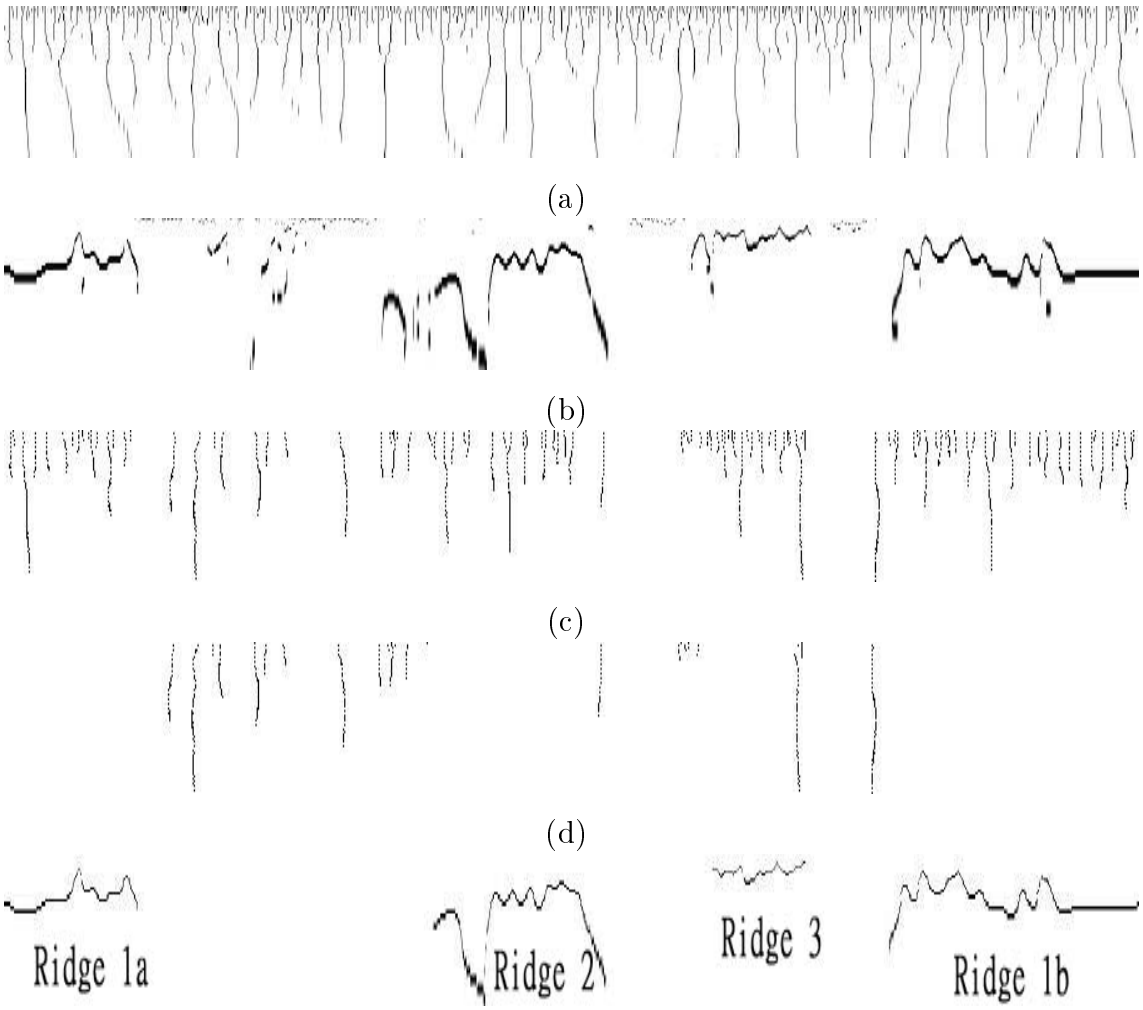

(a) (b) (c) (d) (e)

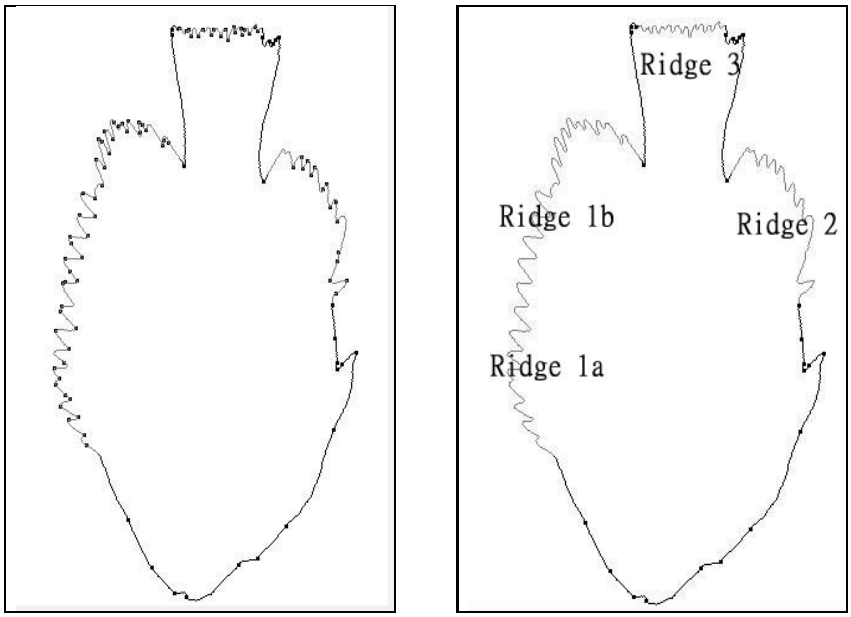

(f) (g)

Figure 5: Shape characterization of a fish. (a) Maxima lines of the singularities. (b) The ridge curves. (c) The remaining maxima lines after removing the maxima lines in (a) which are too short or whose Lipschitz exponents do not indicate the singularities of interest. (d) The maxima lines after removing the maxima lines in (c) which are on the ridges. (e) The remaining ridge curves after deleting short curves. (f) The singular points corresponding to the maxima lines in (c). (g) The singular points corresponding to the maxima line in (d), where the ridge parts are indicated by a light black line.